Fuzzy-Super Twisting Sliding Mode MPPT Control for Three-Phase Grid-Connected PV

Abdellah Ziouh *‡, Ahmed Abbou*

*Department of Electrical Engineering, Mohammadia School of Engineers, Mohamed 5 University, Ibn Sina Street P.B 765, Rabat

(abdellah.ziouh@gmail.com, abbou@emi.ac.ma)

‡Corresponding Author; Abdellah Ziouh, Hassan 2 street number 49, Guelmim, Tel: +212622674121,

abdellah.ziouh@gmail.com

Received: 30.05.2018 Accepted:20.07.2018

Abstract- In this paper, a new fuzzy-super twisting sliding mode control for maximum power point tracking MPPT of a photovoltaic array connected to a three-phase grid is proposed. A voltage source inverter control using d-q components of the grid line currents is employed in order to regulate DC link voltage and also to control the active and reactive injected powers. The effectiveness of the proposed method is demonstrated under standard and real solar insolation and temperature. Additional supplementary power quality control functions as low harmonic distortion rate and zero reactive power injection are ensured. The system performances are simulated under MATLAB/SIMULINK environment.

Keywords Maximum power point tracking; sliding mode; super twisting; three-phasegrid; photovoltaic array; fuzzy logic.

1. Introduction

The gradual increase in the earth's temperature due to greenhouse gases has become one of the most important and difficult problems to solve. In previous years, our planet knew several climate changes and also some dangers natural disasters that caused a huge number of dead people and big losses for governments, for those reasons, renewable energies are gaining more importance and as a result, countries are increasing the injection of these energies into the utility grid in order to decrease the use of fossil fuels. The injected power must be with the possible highest quality (low harmonic rateand zero reactive power) and maximum as possible, so the use of a maximum power point tracking MPPT control becomes very important in order to maximize and stabilize electrical energy delivered by the renewable source (photovoltaic array in our case). In literature, most papers that discuss the grid-connected PV field give more importance to the inverter and d-q components (Synchronous Reference Frame) control in order to ensure the power flow between the DC-DC converter and the three-phase utility grid and to guaranty a robust control of active and reactive power. This strategy makes use of PI controllers in order to control the DC link voltage and for current regulation (inner loop), for MPPT control they use in general a method called perturb and observe P&O due to its simplicity of implementation and its acceptable results [1,2], however, this technique presents oscillations around the maximum power point MPP and it can lose this point during a fast change of irradiation, so to ensure a high quality power flow between the source and grid it is better to use another MPPT technique. [3] Introduced the constant voltage method (CV), which is simple to implement and converges rapidly to the MPP, but the measurement of the open circuit voltage Voc requires the disconnection of the photovoltaic field, which causes energy losses. This problem was solved by the proposal of a technique called pilot cell [4], it has the same principle as CV except that the voltage Voc is measured using an independent photovoltaic cell on the test bench to avoid the loss of energy. A similar algorithm called Constant Current was described in [5] but generally, it has the same disadvantages as the CV method. [6] Proposed an algorithm composed of two modes, the first is InCond which is used at an irradiation greater than 250 W/m², otherwise, the modified constant voltage method MCV is employed. This type of control has a longer delay time due to switching from one mode to another, also it can lose the MPP easily if the climatic conditions vary rapidly. [7] Describes a method that can follow the MPP using power and voltage ripples provided by the solar panel, it can be implemented

analogically using operational amplifiers, however, in terms of rapidity and response time, it still presents some problems.

A method that has attracted the interest of researchers in previous years and has been limited in the control of rotating machines has appeared in the photovoltaic fields, it is the sliding mode and exactly the high order sliding mode control. The power of the sliding mode is in its simplicity of implementation and its robustness against external disturbances [8], it is presenting good results concerning the control of electrical machines and it is well adapted for solar panels when the temperature and the irradiation are varied quickly. The need for a high order sliding mode was appeared because of the problem faced in the first order one, it is chattering around the sliding surface, however, the use of a higher order requires an optimal choice of the gains, for this reason a Mamdani fuzzy controller based on fuzzy logic theorem [9,10] and new rules table is used to optimize the gain β of the second order sliding mode, super twisting, the gain α was chosen to be constant in order to reduce the response time of the system.

The objective of this paper is to present a new method that combines the advantages of sliding mode and artificial intelligence in order to maximize the energy produced by a photovoltaic array connected to a three-phase grid and to overcome the drawbacks of other MPPT techniques.

2. The Studied System

The studied system, showed in Fig.1, is formed by two parts:

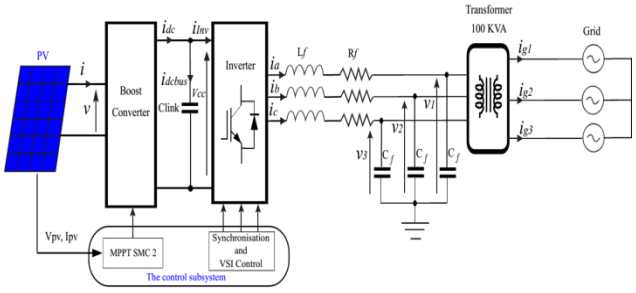

Fig. 1. The studied system.

The power subsystem formed by the PV array, boost converter, three-level inverter, LC filter, 100KVA transformer and the three-phase grid, the main advantages of this topology compared to the single stage inverter are:

- The simplicity of the control and consequently a low response time.
- LC filter with lower inductance and capacitance values.

The second part is the control subsystem formed by two blocks:

Maximum power point tracking (MPPT): controls the photovoltaic array to deliver its maximum power.

Synchronization and VSI (Voltage Source Inverter) control:use a d-q configuration (inner and outer loops, PLL and Park transformation) in order to regulate the DC link voltage and control the active and reactive power injected into the three-phase grid.

3. Modeling of the System Components

3.1. Photovoltaic panel

The PV array is formed by a set of photovoltaic cells coupled in series, its role is to produce electricity when it is exposed to sunlight, so the principal function of the system is to inject the electrical power produced, which depend on the climatic conditions, into the three-phase utility grid. The PV modeling is based on the following equations [11], the electrical model of a photovoltaic cell is presented in Fig.2 [12].

$$Ipv = Iph - Id - \left(\frac{Vpv + Rs \times Ipv}{Rp}\right) \quad (1)$$

$$Iph = (Isc,stc + Kt \times \Delta T)\frac{G}{Gstc} \quad (2)$$

$$Id = Irsc\left(\exp\left[\frac{q(Vpv + Rs \times Ipv)}{A \times Ns \times K \times T}\right] - 1\right) \quad (3)$$

$$Irsc = Irsc,ref\left(\frac{T}{Tref}\right)^3\left(\exp\left[\frac{q \times Eg}{A \times K}\left(\frac{1}{Tref} - \frac{1}{T}\right)\right]\right) \quad (4)$$

$$Irsc,ref = \frac{Isc,stc}{\exp\left(\frac{q \times Voc,stc}{A \times Ns \times K \times T}\right) - 1} \quad (5)$$

$$\Delta T = T - Tref \quad (6)$$

T is the junction temperature in Kelvin (k).
Iph is the light-generated current.
Id is the current passed through the diode.
Irsc, Irsc,ref is reverse saturation current of the diode and reverse saturation current at *Tref*, respectively.
Isc, Isc,stc are the short-circuit current and the open-circuit voltage at standard test conditions STC (Gstc = 1000W/m², *Tref* = 25C° and AM 1.5), respectively.
Kt is short-circuit current temperature coefficient.
G is the real irradiation.
Ns is the number of cells in series.
Rs is the series resistance.
Rp is the parallel resistance.
Eg is silicon energy gap.
K is Boltzmann's constant.
A is the ideality factor.
q is the electron charge.

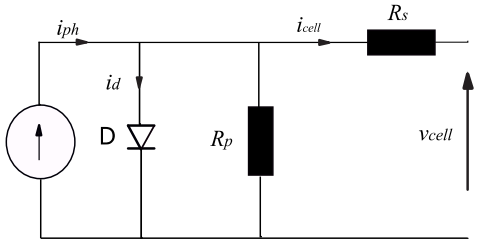

Fig. 2. Photovoltaic cell model.

The PV array is constituted by 100 photovoltaic panels associated in parallel, each has an output power of 320W, so the total produced power is 32KW.

3.2. Boost DC-DC converter

The boost converter has an important role in the studied system, it controls the PV array output power in order to reach the maximum power point. This strategy is based on an MPPT technique (Fuzzy-Super twisting control) which adjusts the duty cycle *d* of the boost converter [13], Fig. 4, in order to make the PV voltage converge towards the Vmpp value, Fig. 3 [14].

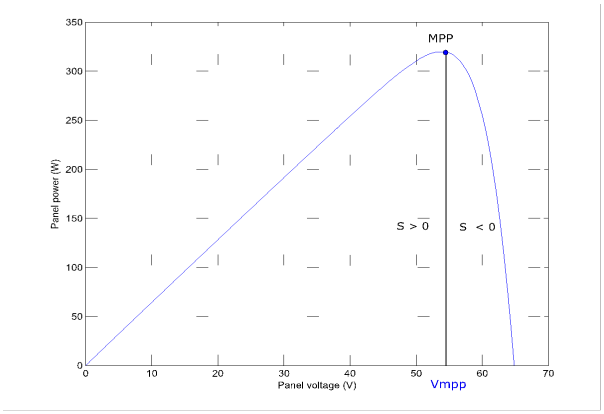

Fig. 3. P(V) characteristic of a PV panel.

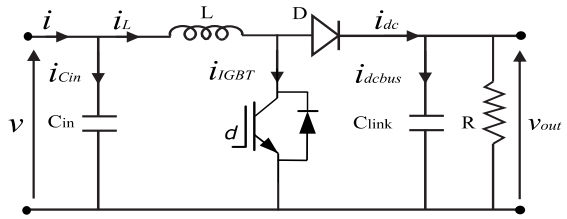

Fig. 4. Boost converter.

If d=1 (Fig.5): *iL=iIGBT*

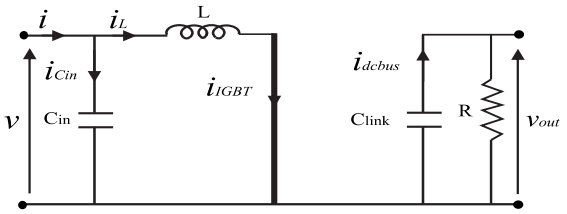

Fig. 5. Boost converter when d=1

$$v = L\frac{diL}{dt} \tag{7}$$

$$\frac{-vout}{R} = Clink\frac{dvout}{dt} \tag{8}$$

If d = 0 (Fig.6): *iL = idc*

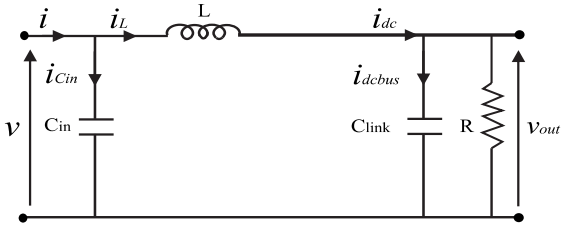

Fig. 6. Boost converter when d=0

$$v - v_{out} = L\frac{diL}{dt} \tag{9}$$

$$iL - \frac{v_{out}}{R} = C_{link}\frac{dv_{out}}{dt} \tag{10}$$

3.3. Inverter

The inverter used is a three-level one, its role is to convert the input current and voltage (iInv and Vcc) to an alternative form, in general, this topology of inverters presents more advantages compared to the two-level one, it limits the harmonic currents and generates more stable power, however to guarantee the injection of a stable active power to the three-phase grid, an LC filter must be used. A 100 KVA transformer is used for the adaptation of the inverter output voltage with that of the three-phase medium-voltage grid (25 KV). According to Fig. 4, the photovoltaic array output power and current can be described by:

$$p = v.i \tag{11}$$

$$i = i_{Cin} + i_{IGBT} + i_{dc} \tag{12}$$

The boost output current can be written as follow:

$$i_{dc} = i_{dcbus} + i_{Inv} \tag{13}$$

Where
v, i are the photovoltaic array output voltage and current, respectively.
p is the available power for specific climatic condition.
iCin is the current through the boost input capacitor.
iIGBT is the current passed through the IGBT transistor.
idc is the boost output current.
idcbus is the current through the DC link capacitor and
iInv is the inverter input current.

The phase-neutral voltage in the LC filter capacitor is the same as the phase-neutral voltage of the three-phase grid, so we can deduce the dynamics expression of the AC inverter side.

$$v - v' = R.i + L\frac{di}{dt} \tag{14}$$

$$\begin{bmatrix} va \\ vb \\ vc \end{bmatrix} - \begin{bmatrix} v1 \\ v2 \\ v3 \end{bmatrix} = R\begin{bmatrix} ia \\ ib \\ ic \end{bmatrix} + L\frac{d}{dt}\begin{bmatrix} ia \\ ib \\ ic \end{bmatrix} \tag{15}$$

Where ***v***,***i*** and ***v'*** are the phase-neutral inverter voltage, the inverter output current and the grid phase-neutral voltage space vectors.

In order to control the instantaneous active and reactive power injected to the three-phase grid, we must analyze the three-phase system (voltages and currents) in the rotating synchronous reference frame which uses the d-q component deduced by a Park transformation. For a three-phase system described by vector$y = [y1,y2,y3]$, where ***y1***, ***y2***, and ***y3*** are the three-phase variables, a Park vector frame is obtained with a Clarke transformation plus a rotation with an angle equal to the utility grid voltage phase angle, the Clark transformation is defined as follows:

$$\begin{bmatrix} y0 \\ y\alpha \\ y\beta \end{bmatrix} = \sqrt{\frac{2}{3}} \begin{bmatrix} \frac{1}{\sqrt{2}} & \frac{1}{\sqrt{2}} & \frac{1}{\sqrt{2}} \\ 1 & -\frac{1}{2} & -\frac{1}{2} \\ 0 & \frac{\sqrt{3}}{2} & -\frac{\sqrt{3}}{2} \end{bmatrix} \begin{bmatrix} y1 \\ y2 \\ y3 \end{bmatrix} \tag{16}$$

The Park or d-q components are deduced by a rotation:

$$\begin{bmatrix} yd \\ yq \end{bmatrix} = \sqrt{\frac{2}{3}} \begin{bmatrix} \cos\theta & \sin\theta \\ -\sin\theta & \cos\theta \end{bmatrix} \begin{bmatrix} y\alpha \\ y\beta \end{bmatrix} \tag{17}$$

The instantaneous active and reactive power ***p*** and ***q***, respectively:

$$\begin{aligned} p &= v'd.id + v'q.iq \\ q &= v'q.id - v'd.iq \end{aligned} \tag{18}$$

Where *id*, *iq*, *v'q* and *v'q* are the d-q components of the three-phase grid currents and voltages, respectively, if vector *v'q*equal zero (aligned with the d axis) we can ensure a separate control of the instantaneous active and reactive powers.

$$\begin{aligned} p &= v'd.id \\ q &= -v'd.iq \end{aligned} \tag{19}$$

In order to have a zero error at the steady state, a PI regulator is used due to the continuous nature of d-q components.

The control subsystem is formed by a Maximum Power Point Tracking (MPPT) block, a three-phase voltage source inverter control (VSIC), Fig. 7, that is composed of an inner and an outer loop and finally, a phase-locked loop (PLL) and a Pulse Width Modulation PWM block.

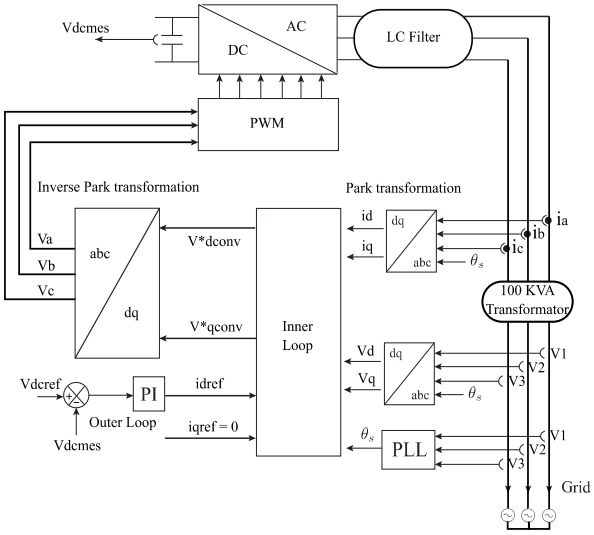

Fig. 7. Three-phase voltage source inverter control (VSIC)

Maximum Power Point Tracking: This block is used to control the DC-DC boost converter in order to make the PV panel delivers the maximum power available in specific climate conditions (temperature and irradiation). A fuzzy-super twisting MPPT control that combines a second order sliding mode and a Mamdani-fuzzy logic is discussed in the fifthparagraph.

Three-phase voltage source inverter control (VSIC):

Inner loop: The inner loop, Fig. 8, is formed by two PI controllers in order to regulate the d-q components of the line currents so to control the instantaneous active and reactive powers injected into the three-phase utility grid. By using the Park transformation the measured three-phase grid voltages and inverter output currents are presented in the rotating synchronous reference frame (d-q reference).

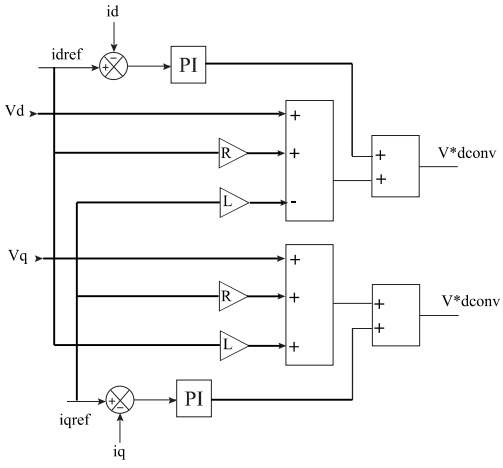

Fig. 8. Inner loop for current regulation.

The id component is compared to idref the output of the outer loop in order to control the active power p, on the other hand, the iq component is set to zero (i_{qref}=0) for a zero reactive power (q=0) injected into the utility grid, the coefficient ki and kp of the PI regulator can be calculated as follows [15], [16]:

$$\frac{ki}{kp} = \frac{2\pi fc}{\tan\left(-90° + P_{Mg} + \tan^{-1}(2\pi f_c \tau)\right)} \quad (20)$$

$$kp = \frac{F_{sr}}{G_{inv}} \frac{1}{K_{ct}} \frac{L}{\tau} \sqrt{\frac{1+(2\pi fc\tau)^2}{1+\left(\frac{1}{2\pi fc}\frac{ki}{kp}\right)^2}} \quad (21)$$

Where
fc is the crossover frequency of the inner loop.
PMg is the phase margin.
τ is the time constant.
Fsr is the full-scale range which is set to 1.
***Ginv* = 2Vcc/3** is the gain of the inverter.
Kct is the gain of the current transducer it is set to 1.
Vcc = 500 VDC is the DC bus voltage.

Outer loop: The outer loop, Fig. 7, is formed by one PI regulator which controls the DC bus voltage and keeps it equal to the reference,so the power flow between the photovoltaic array and the three-phase utility grid is ensured.

Phase locked loop: *PLL*

It calculates the phase angle of the three-phase grid voltage which is necessary for Park transformation and also to synchronize the inverter output voltage with that of the three-phase utility grid.

Pulse Width Modulation:

The inner loop generates the reference d-q components of the inverter output voltages, these two components transformed to the three-phase frame, by an inverse Park transformation, are the inputs of a PWM block which controls the commutation of the inverter switchers in order to follow the reference voltage.

3.4. LC filter

The LC filter is a second-order low-pass filter whose function is to attenuate the harmonic currents generated at the AC side of the inverter due to the high-frequency commutation of IGBTs and make the harmonic distortion rate less than 5% [16].

There are three filter topologies commonly used in literature, the L, LC, and LCL, however, the LC one has a further attenuation of the switching frequency because of the addition of a shunt capacitor that ensures a deeper attenuation (-40 dB per decade) compared to the L filter (-20 dB per decade).

The LCL filter ensures more reduced harmonic amplitude because of the addition of another inductance, but its entire inconvenient is the distortion of the input current due to resonance effect, so for that reason, we chose an LC topology. The resonant frequency equal:

$$f_0 = \frac{1}{2\pi}\frac{1}{\sqrt{LC}} \quad (22)$$

The harmonic standard allows a 15-20% of the rated current [17], so the inductor value can be calculated by (23), the main parameters are mensionned in table 1.

$$L = \frac{1}{6}\frac{\delta}{\Delta iL}\frac{V_{dc}}{f_s} \quad (23)$$

L is the filter inductor.
Vdc is the DC link voltage.
fs is the switching frequency.
δ that is the maximum duty cycle equal to 75%.

Table 1: Parameters values

Parameter	Value
Solar panel (for each panel)	
Rs	0.2365 Ohm
Rp	415.405 Ohm
Kt	0.0035 A/K°
G	1000 W/m²
Ns	96
K	$1{,}3805.10^{-23}$ J/K°
A	1.4
Eg	1.12
q	$1{,}6201.10^{-19}$ C
Boost converter	
Cin	100.10^{-6} F, the PV array is formed by 100 panels in parallel, so a low voltage at the boost input
Clink	2 capacitances of 83F, the DC link voltage is 500 VDC, so we need a very high capacitance value
L	5.10^{-3} H
LC Filter	
L	850.10^{-6} H
C	1,34 F

4. Sliding Mode

The sliding mode was introduced for the first time in the literature by [18] and [19] in the 1960s years of old Union of Soviet Socialist Republics for variable structure systems. In the last years, an increasing interest for sliding mode was

appeared due to its simplicity of elaboration, robustness against external disturbances and parameter incertitude. The principle of this technique is to constrain the system to reach and then stay on a given surface. The considered surface is then designated as the surface of switching. The resulting dynamic behavior, called ideal sliding regime, is completely determined by the parameters and equations defining the surface. The advantages of this type of control are:

- Reduction of the system order
- The sliding regime is robust against disturbances occurring in the same directions as the inputs (matching disturbances)

The sliding mode control is generating on two steps:

- Choice of the sliding surface
- Determination of control law

4.1. First order sliding mode

4.1.1. Choice of the sliding surface

Let a nonlinear system, refined in the entry, defined by:

$$\dot{x} = f(x(t),t,u(t)) \tag{24}$$

Where:

$u : R^n \to R$ is the input and $x = [x1,...,xn] \in X$

X is a differentiable manifold, either open set of R^n

f and g are space vector differentiable and defined on Xs a differentiable function called the sliding function:

$s : X \times R^+ \to R$

As $\frac{\partial s}{\partial x} \neq 0$ on X

The set $S = \{x \in X : s(t,x) = 0\}$ called sliding or switching surface.

Note:

The systems studied in this paper contain discontinuous terms, so the classical theory of differential equations does not allow finding solutions, so we must refer to the theory of differential inclusions and solutions in Filippov's sense.

An ideal sliding mode exists on S if: $\exists ts$ as $s(t,x) = 0$ $\forall t \geq ts$

In another way if :

$$\lim_{s \to 0^+} \frac{\partial s}{\partial x}(f) < 0 \text{ and } \lim_{s \to 0^-} \frac{\partial s}{\partial x}(f) > 0$$

This means that the velocity vectors of the system's trajectories converge to the sliding surface.

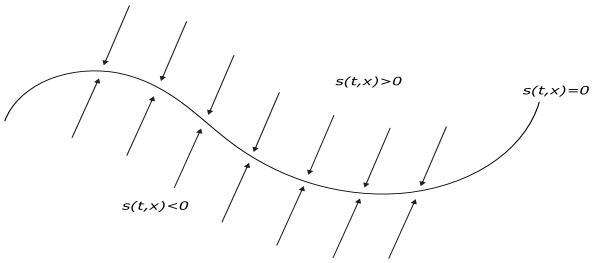

Fig. 9. The space state and sliding surface .

From this definition, we deduce that the objective of the first order sliding mode is to make S= 0. Sliding mode exists if the surface is attractive otherwise if the following condition is verified:

$$\dot{s} \cdot s < 0$$

4.1.2. Determination of the control law

The control law is formed by two components: Firstly the reaching law [20] component:

Constant reaching law:

$$ur = -\beta sign(S) \tag{25}$$

Constant proportional reaching law:

$$ur = -\beta sign(S) - k.S \tag{26}$$

Power reaching law:

$$ur = -k|S|^{\alpha} sign(S) \tag{27}$$

Secondly, the equivalent law component determined from the invariance condition:

$$\begin{cases} s = 0 \\ \dot{s} = \frac{\partial s}{\partial x}\left[f(x) + g(x)ueq\right] = 0 \end{cases} \tag{28}$$

4.1.3. Chattering phenomenon

The ideal sliding regime does not exist because of the limitation of the electronic components in terms of frequency, they cannot operate at an infinite frequency, so the operating point oscillates around s(t,x) = 0.

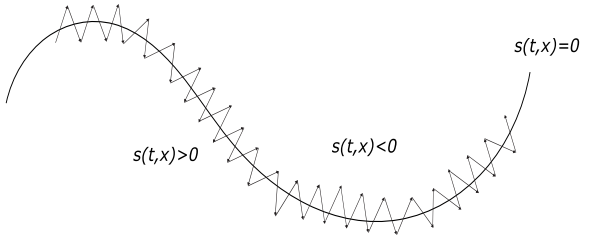

Fig. 10. Chattering phenomenon.

This problem causes vibrations in electrical machines, energy losses and a delay in response time. Among the

solutions used to avoid this problem, we find the use of functions other than Sign to filter the high-frequencycomponent,however, the use of a higher order is the most useful solution.

4.1.4. Second order sliding mode: Super twisting

The sliding mode exists on the manifold S in the neighborhood of a sliding point of order n, if in the manifold of this point the set Sr is composed of trajectories in Filippov's sense.

$$Sr = \left\{ x \in X : s = \dot{s} = ... = s^{r-1} = 0 \right\}$$

The control law u is an n order ideal sliding mode algorithm on the manifold S, if u generates an n order sliding mode on S, i.e.:

$$s = \dot{s} = ... = s^{r-1} = 0 \tag{29}$$

Consider the system define by equation (24),assume that f and s are respectively, C^1 and C^2 functions and the only available informationsare the current values of u(t), s(x,t) and t, the second order control law ensures the following condition in a finite time:

$$s = \dot{s} = 0$$

In order to define the control law the following hypothesis must be considered [21]:

- $U = \{u : |u| \le Um\}$ where $Um > 1$ is a real constant.
- $\exists u' \in [0,1]$ such that $\forall u(t)$ with $|u(t)| > u'$, $\exists t_1$ such that $s(t)u(t) > 0$ for $t > t_1$.
- There are positive constants s0, u"<1, km and kM such that if $|s(x,t)| \le s_0$ then:

$$km \le \frac{\partial}{\partial u}\dot{s}(x,t,u) \le kM \;\; \forall u \in U, \forall x \in X$$

and $|u| > u''$ entails $u \cdot \dot{s} > 0$

- $\exists \phi > 0$ such that $\forall t, \forall x \in X, \forall u \in U$ then :

$$\left| \frac{\partial}{\partial t}\dot{s}(x,t,u) + \frac{\partial}{\partial x}\dot{s}(x,t,u) f(x,t,u) \right| \le \phi$$

Where $\dot{s}(x,t,u)$ is the total time derivative of the sliding function s, defined as:

$$\dot{s} = \dot{s}(x(t),t,u(t)) = \frac{\partial}{\partial t}s(x,t) + \frac{\partial}{\partial x}s(x,t) f(x,t,u) \tag{30}$$

The sliding mode has been introduced for systems with relative degree one in order to solve the chattering problem in variable structure systems. The trajectories on the 2-sliding plane has a twisting form around the origin and the control law$u$is constituted by three components, one is defined by its time derivative, the second is a continuous function of sliding variable and the third is the equivalent law [22].

$$\begin{cases} u(t) = u_1(t) + u_2(t) + u_{eq} \\ \dot{u}_1(t) = -\alpha sign(S) \\ u_2(t) = -\beta |S|^{\rho} sign(S) \end{cases} \tag{31}$$

The sufficient conditions ensuring a finite time convergence to the sliding surface are [23]:

$$\begin{cases} \alpha > \dfrac{\phi}{km} \\ \beta^2 \ge \dfrac{4\phi}{km^2} \dfrac{kM(\alpha+\phi)}{km(\alpha+\phi)} \\ 0 < \rho \le 0.5 \end{cases} \tag{32}$$

Where ***α, β, Ø, km, kM***,and ***ρ*** are positive constants. The main advantage of the super –twisting compared to other second order algorithms is that the evaluation of the sign of time derivative of the sliding surface is not necessary.

5. Fuzzy Logic Optimization Controller

The fuzzy logic optimization controller proposed in this paper is based on the fuzzy set theorem which was developed and proposed for the first time by Lotfi Zadeh in 1965 [24]. The model used is a Mamdani [25] one and it is based on new rules and membership functions in order to optimize the gain β. The operating principle of this regulation is to convert input variables to linguistic ones, this makes the fuzzy logic controller more suitable for nonlinear systems and systems with uncertain input variables. The fuzzy controller proposed [26] in Fig. 11 is used to generate the optimal super twisting gain β. With this controller we can adjust easily β and fix the other one α in order to have more simple structure (one parameter) compared to conventional optimization methods which adjust the two gains in the same time.

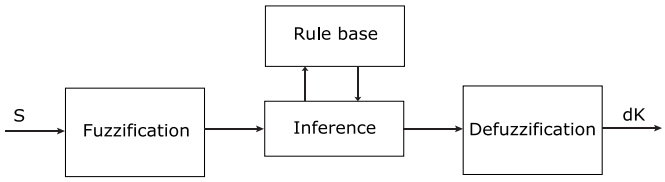

Fig. 11. Fuzzy logic controller.

This controller is constituted from the following steps:

Fuzzification: Converts numeric input variable that is S (sliding surface) to a linguistic one using membership functions, Fig. 12.

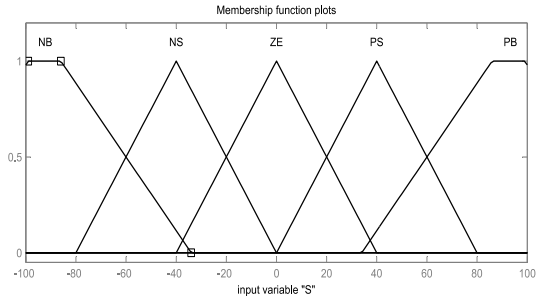

Fig. 12. Fuzzification membership functions.

Inference: Generates other linguistic variables using the outputs of the previous step and a rules table as depicted in table 2.

Table 2: Rules Table

Sliding surface S	Step dK
If S is NB	ΔK is PB
If S is NS	ΔK is PS
If S is ZE	ΔK is ZE
If S is PS	ΔK is PS
If S is PB	ΔK is PB

Defuzzification: This block converts a fuzzified variable into a single crisp value that is the step of increasing or decreasing of the gain β using a mathematical method called the mean of maxima. With this method, the defuzzified value is calculated by equation (33), defuzzification membership functions are illustrated in Fig. 13.

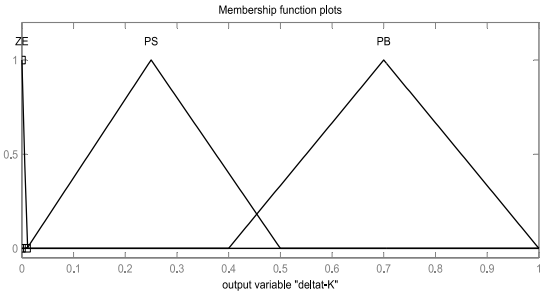

Fig. 13. Defuzzification membership functions.

Let f(x) a membership of the fuzzy set B, x∈X, where X is a universe of discourse. The crisp value or the defuzzification output is:

$$x' = \frac{\sum_{xi \in M} xi}{|M|} \tag{33}$$

M={xi | f(xi) is equal to the height of the set B } and $|M|$ is the cardinality of M.

6. Fuzzy Logic Optimization Controller

6.1. The system under standard test conditions:

MATLAB/SIMULINK environment has been used to simulate the studied system and to illustrate its behavior in standard and reel climatic conditions. This paragraph presents the simulation results in standard test conditions (irradiation = 1000 W/m², temperature = 25C° and 1.5 AM). Fig. 14 shows the PV array output power using the proposed fuzzy-super twisting MPPT control, it is clear that the power reaches its maximum value that is 32 kW (100 panels of 320 W each).

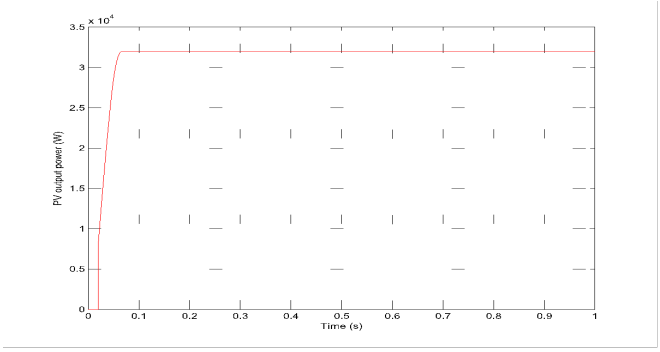

Fig. 14. PV array output power.

In general, most grid-connected PV application uses the P&O method for MPPT control, but its main disadvantage is oscillations around the maximum power point which causes energy losses, however with the proposed MPPT technique the PV array output power is more stable and arrives at the MPP in a short response time and with high accuracy.

Three-phase currents injected into utility grid are presented in Fig. 15, they have 50 Hz in frequency and a sinusoidal waveform which ensures a low current harmonics rate. The three-phase grid voltages have also a sinusoidal waveform ensuring a low voltage harmonics rate as depicted in Fig. 16.

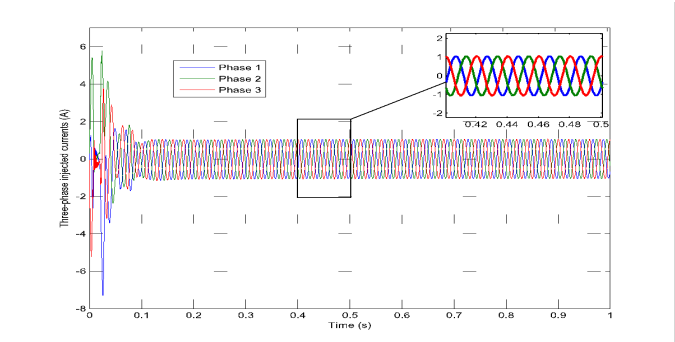

Fig. 15. Three-phase injected currents (the transformer secondary).

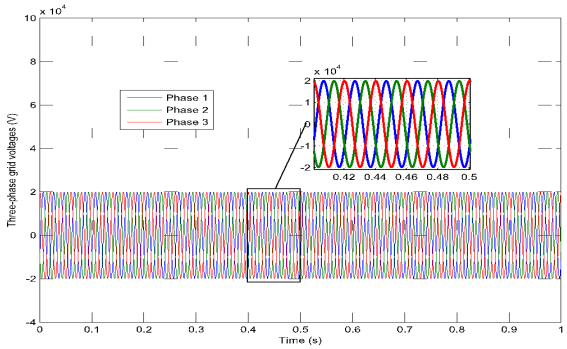

Fig. 16. Three-phase grid voltages (the transformer secondary).

These two figures illustrate also that the grid voltages and currents are in phase, which confirms that no reactive power injected into the grid.

Fig. 17 shows the instantaneous active and reactive power, respectively, injected into the utility grid, the active power is around 32 KW which is the maximum power delivered by the PV array, reactive power equal zero.

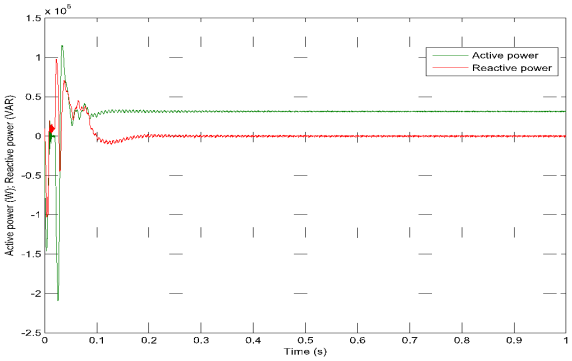

Fig. 17. Instantaneous active and reactive power injected into the grid.

DC link voltage tracks exactly the reference value 500 V as depicted in Fig. 18. The dynamics of the sliding surface and its time derivative are shown in Fig. 19 and Fig. 20.

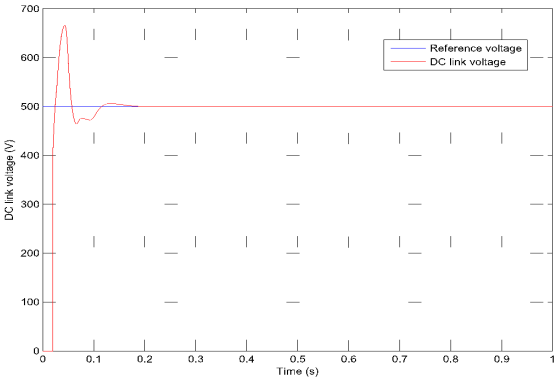

Fig. 18. DC link voltage.

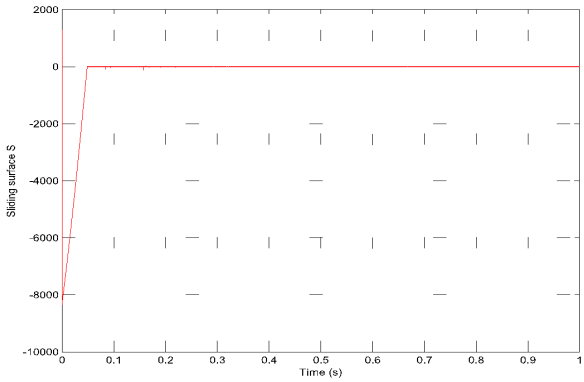

Fig. 19. The dynamics of the sliding surface S.

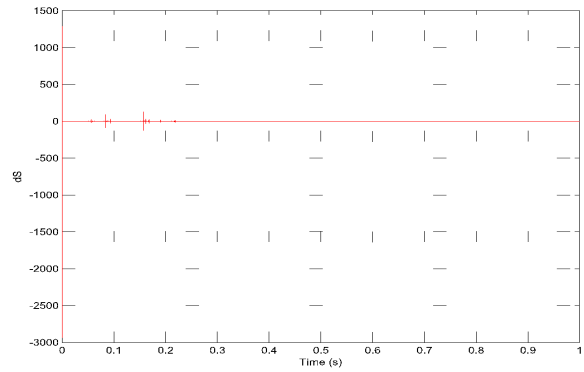

Fig. 20. The dynamics of the time derivative of the sliding surface.

6.2. The system under reel climatic conditions:

This section discusses the results of simulation under variable climatic conditions, Fig. 21 and Fig. 22 present, respectively, the profile of irradiation and temperature used.

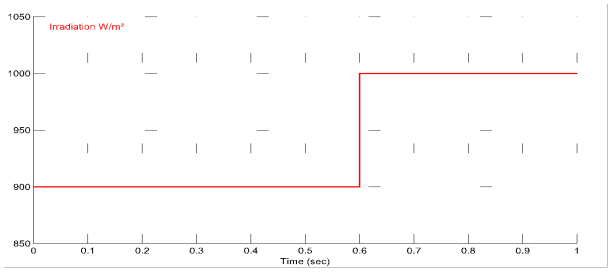

Fig. 21. Irradiation profile in W/m².

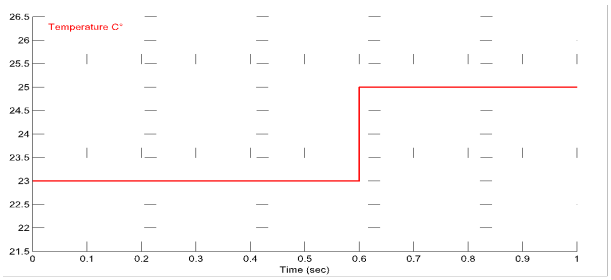

Fig. 22. Temperature profile in C°.

Generally, irradiation and temperature are not constant, for that reason it is necessary to simulate the system in reel

climatic conditions in order to analyze the behavior of the fuzzy-super twisting MPPT algorithm. Fig. 23 shows clearly the convergence of the PV array output power to the maximum value, each time the irradiation and temperature changed the power tracks the MPP with a high accuracy. The PV output voltage tracks the Vmpp value as depicted in Fig. 24, this low value is justified by the structure on panels are associated, they are all connected in parallel form.

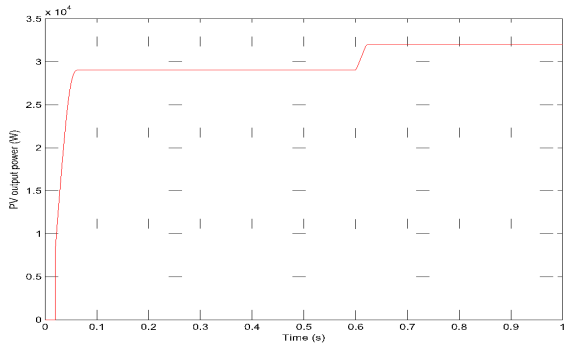

Fig. 23. PV output power under variable climatic conditions.

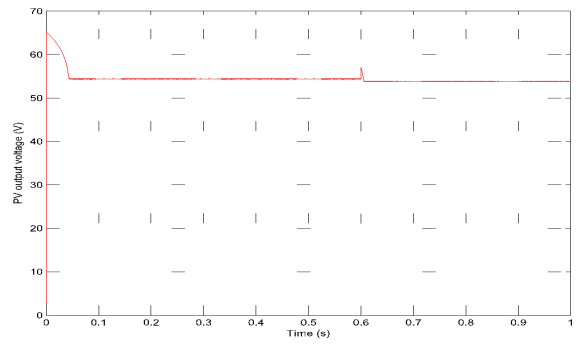

Fig. 24. PV output voltage.

In order to guarantee a high-quality power flow from the renewable source into the three-phase grid, the DC link voltage is regulated by an outer loop to track the reference value which is 500 V. Fig. 25 presents the dynamics of the DC link voltage compared to the reference value, it is clear that despite the variation of irradiation and temperature the inverter input voltage tracks exactly and in a low response time the reference value (500 V).

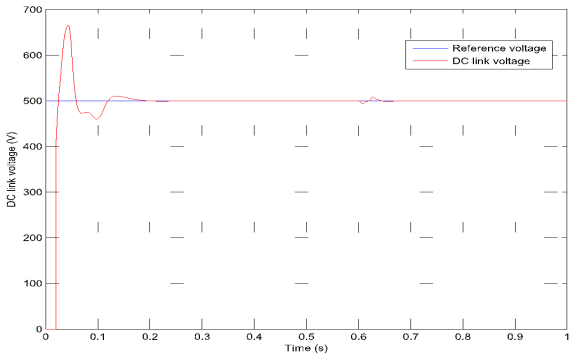

Fig. 25. DC link voltage .

Active power injected into the utility grid is less from the PV output power due to DC-DC boost and inverter losses as depicted in Fig. 26, it depends on climatic changes. The same figure shows that reactive power injected is null.

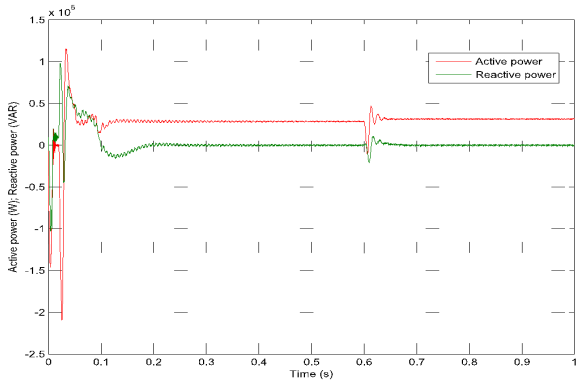

Fig. 26. Instantaneous active and reactive power injected into grid.

The VSI control uses a PLL block to detect the phase angle of the utility grid voltages in order to synchronize them with that at the inverter output. Fig. 27 and Fig. 28 illustrate the three-phase grid currents and voltages, respectively. Fig. 29 shows the first phase current and voltage. From these figures, the expected performances have been approved either in the zero reactive power injected into the grid and the unit power factor, voltage and current in phase, or in current and voltage harmonic rate which is very low, thing that is clear from the sinusoidal waveform. At the instance 0.6s the temperature and irradiation changed so the current amplitude becomes higher, due to the increase in the PV output power, voltages are constant and synchronized with that of the grid.

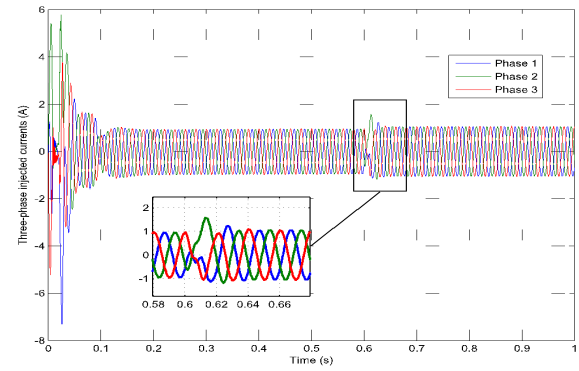

Fig. 27. Three-phase injected currents(the transformer secondary).

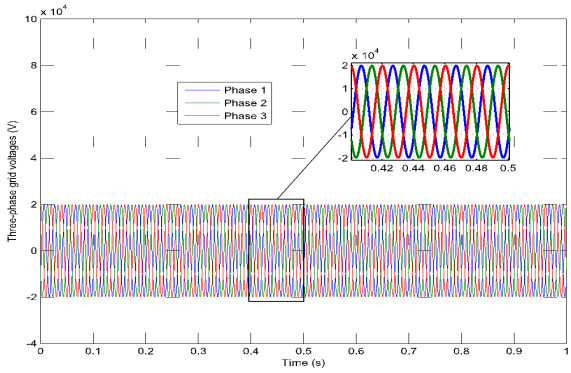

Fig. 28. Three-phase grid voltages (the transformer secondary).

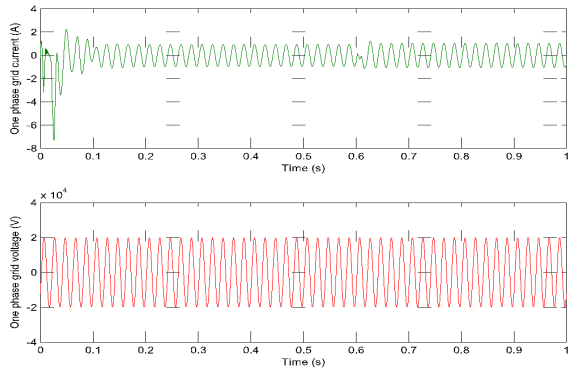

Fig. 29. One phase grid voltage and current (the transformer secondary).

7. Conclusion

In this paper, a fuzzy super-twisting technique has been used in order to maximize the energy delivered by a photovoltaic array connected to a three-phase utility grid. A fuzzy logic controller based on new rules table and membership functions has been proposed to adjust one gain of the second-order sliding mode, super twisting, control law. On the DC side, the PV output power has tracked the maximum power with a high accuracy in a short response time and with low ripples in standard and reel climatic conditions. On the AC side, the injected three-phase currents into grid have a sinusoidal waveform so a low harmonics distortion rate and they are in phase with the three-phase grid voltages which ensures the injection of a null reactive power. The proposed method can be implemented experimentally using a dSPACE hardware and it can give more efficient results if we use an active filter instead of the LC one.

References

[1] B. Subudhi and R. Pradhan, "A Comparative Study on Maximum Power Point Tracking Techniques for Photovoltaic Power Systems", IEEE Trans Sustain Energy, Vol. 4, No. 2, pp. 89–98, 2013.

[2] L. Xingshuo, W. Huiqing, and H. Yihua, "Evaluation of Different Maximum Power Point Tracking (MPPT) Techniques based on Practical Meteorological Data", 5th IEEE International Conference on Renewable Energy Res earch and Applications, Birmingham, UK, pp. 696-701, 20-23 November 2016.

[3] N. Hyeong-Ju, L. Dong-Yun, and H. Dong-Seok, "An improved MPPT converter with current compensation method for small scaled PV-applications", 28th Annual Conference of the IEEE Industrial Electronics Society Conference, Sevilla, pp. 1113-1118, 5-8 November 2002.

[4] ZM. Salameh, F. Dagher, and WA. Lynch, "Step-down maximum power point tracker for photovoltaic systems", Sol Energy, Vol. 46, No. 5, pp. 279-282, 1991.

[5] SM. Alghuwainem, "Matching of a dc motor to a photovoltaic generator using a step-up converter with a current-locked loop", IEEE Trans Energy Convers, Vol. 9, No. 1, pp. 192-198, 1994.

[6] G.J. Yu, Y.S. Jung, J.Y. Choi and G.S. Kim, "A novel two mode MPPT control algorithm based on comparative study of existing algorithms", Solar Energy, Vol. 76, pp. 455–463, 2004.

[7] RK. Nema and P. Bhatnagar, "Maximum power point tracking control techniques: state-of-the-art in photovoltaic applications", Renew Sustain Energy Review, Vol. 23, pp. 224-241, 2013.

[8] A. Del Pizzo, L.P. Di Noia, and S. Meo, "Super Twisting Sliding mode control of Smart-Inverters grid–connected for PV Applications", 6th IEEE International Conference on Renewable Energy Research and Applicat ions, San Diego, USA, pp. 793-796, 5-8 November 2017.

[9] AI. Dounis, P. Kofinas, C. Alafodimos and D. Tseles, "Adaptive fuzzy gain scheduling PID controller for maximum power point tracking of photovoltaic system", Renew Energy, Vol. 60,pp. 202-214, 2013.

[10] MM. Algazar, H. Al-Monier, HA. EL-halimand M. Salem, "Maximum power point tracking using fuzzy logic control", International Journal of Electrical Power Energy Systems, Vol. 39, No. 1, pp. 221-228, 2012.

[11] M.G. Jaboori, M.M. Saied, and A.A. Hanafy, "A contribution to the simulation and design optimization of photovoltaic systems", IEEE Tans Energy Conv, Vol. 6, pp. 401-406, 1991.

[12] A. Zaidi, K. Dahech, T. Damak, "Maximum Power Point Tracking of Photovoltaic Systems Based on Fast Terminal Sliding Mode Controller", International journal of renewable energy research, Vol. 6, No. 4, 2016.

[13] H. Sahraoui, L. Chrifi-Alaoui, S. Drid, and P. Bussy, "Second Order Sliding Mode Control of DC-DC Converter used in the Photovoltaic System According an Adaptive MPPT", International journal of renewable energy research , Vol. 6, No. 2, 2016.

[14] K. Kajiwara, N. Matsui, and F. Kurokawa, "A New MPPT Control for Solar Panel under Bus Voltage Fluctuation", 6th IEEE International Conference on Renewable Energy Research and Applications" San Diego, USA, pp. 1047-1050, 5-8 November 2017.

[15] A.B. Rey-Boué, R. García-Valverde, F. de A. Ruz-Vila and J.M. Torrelo-Ponce, "An integrative approach to the design methodology for 3-phase power conditioners in Photovoltaic Grid-Connected systems", Energy Conversion and Management, Vol. 56, pp. 80-95, 2012.

[16] S. Buso and P. Mattavelli, Digital Control in Power Electronics, Morgan & Claypool, 2006.

[17] IEEE Standards 519, "Recommended Practices and Requirements for Harmonic Control in Electric Power Systems", 1992.

[18] D.V. Anosov, "On stability of equilibrium points of relay systems", Automation and remote control, Vol. 2, pp. 135-149, 1959.

[19] S.V. Emel'yanov, "On pecularities of variable structure control systems with discontinuous switching functions", Doklady ANSSR, Vol. 153, pp. 776-778, 1963.

[20] W. Gao and J.C. Hung, "Variable structure control of nonlinear systems: a new approach", IEEE Tran Ind Electron, Vol. 40, pp. 45-55, 1993.

[21] Pisano, "Second Order Sliding Modes: Theory and Applications", Dipartimento di Ingegneria Elettrica ed Elettronica (DIEE), Università degli Studi di Cagliari, 2000.

[22] Evangelista, P. Puleston, F. Valenciaga, L.M. Fridman, "Lyapunov-designed super-twisting sliding mode control for wind energy conversion optimization", IEEE Trans Indust Electron, Vol. 60, No. 2, pp. 538–545, 2013.

[23] Bouafassa, L. Rahmani, S. Mekhilef, "Design and real-time implementation of single-phase boost power factor correction converter", ISA Trans, Vol. 55, pp. 267–274, 2015.

[24] L.A. Zadeh, Fuzzy sets, vol. 8. Information *and* Control, 1965, pp. 338 – 353.

[25] E.H. Mamdani and S. Assilian, "An experiment in linguistic synthesis with a fuzzy logic controller", Intern. J. Man-Machine Stud, Vol. 7, pp. 1–13, 1975.

[26] M. A. Abdourraziq and M. Ouassaid, M. Maaroufi, "Single-Sensor Based MPPT for Photovoltaic Systems", International journal of renewable energy research , Vol. 6, No. 2, 2016.